Turkish Journal of Electrical Engineering & Computer Sciences

http://journals.tubitak.gov.tr/elektrik/

Research Article

Turk J Elec Eng & Comp Sci
(2019) 27: 2526 – 2540

doi:10.3906/elk-1804-38

QPSK-dual carrier modulation for ultra-wideband communication in body area network channels

Yasin KARAN[1], **Salim KAHVECİ**[2*]

[1]Department of Physics, Faculty of Art and Science, Recep Tayyip Erdoğan University, Rize, Turkey
[2]Department of Electrical and Electronics Engineering, Faculty of Engineering, Karadeniz Technical University Trabzon, Turkey

Received: 16.04.2018 • **Accepted/Published Online:** 08.05.2019 • **Final Version:** 26.07.2019

Abstract: Dual carrier modulation (DCM) using orthogonal frequency-division multiplexing (OFDM) improves the performance in multipath fading channels. In the literature DCM is proposed with 16-quadrature amplitude modulation (16QAM) for ultra-wideband (UWB) communication, with four bits per symbol to keep reliable high date transmission over longer distances. Body area network (BAN) standards address transmission reliability more than data rate. UWB is one of the physical layers proposed in BAN standards. In this study, DCM is used with quadrature phase shift keying (QPSK) instead of 16QAM to have better performance in reliable transmission. The performance of QPSK-DCM is analyzed and compared with 16QAM-DCM, QPSK-OFDM, and 16QAM-OFDM in a wireless body area network channel. These simulation results are given as bit error rate (BER) versus signal to noise ratio per bit (E_b/N_0) graphs. Additionally, derivations of theoretical $BER - E_b/N_0$ performances of QPSK-OFDM and 16QAM-DCM in an additive white Gaussian noise (AWGN) channel are given.

Key words: Dual carrier modulation, wireless body area network channel, orthogonal frequency-division multiplexing

1. Introduction

Ultra-wideband (UWB) is an eligible communication type for low energy consumption and high bandwidth in short range. The Federal Communications Commission (FCC) and the International Telecommunication Union (ITU) defined UWB systems whose bandwidth is greater than 500 MHz or 20% of central frequency in the 3.1 GHz to 10.6 GHz frequency band. The spectral mask defined by the FCC for UWB systems is given in Figure 1. This figure shows emission power limitations based on frequencies for indoor and outdoor mediums. UWB signals should be inside the limits and comply to the mask [1, 2].

Due to the high data rate carrier and low energy consumption features of UWB, it is defined in some communication standards such as ECMA 368, IEEE 802.15.3a, and IEEE 802.15.6. ECMA 368 and IEEE 802.15.3a specify the high data rate in short range communication. Unlike these two standards, IEEE 802.15.6 specifies high quality of service (QoS) because it is a communication standard of a body area network, which has vital importance [3]. ECMA 368 and IEEE 802.15.3a standards use UWB physical layer (PHY) supporting high data rates with multiband orthogonal frequency division modulation (MB-OFDM) [4, 5]. IEEE 802.15.6 offers three PHY: narrowband, ultra-wideband, and human body communications PHYs. IEEE 802.15.6 UWB PHY included impulse radio (IR-UWB) and wideband frequency modulation (FM-UWB). Even though the

*Correspondence: salim@ktu.edu.tr

same wireless technology (UWB) is used in both standards, the IEEE 802.15.6 standard focuses on QoS and reliable data transfer instead of higher data rates [3].

OFDM is a widely used modulation technique because of its immunity to multipath channel effects. Multiple carriers allow carrying more data and a cyclic prefix or guard interval protects interleaving of data symbols. In the UWB systems, the frequency bandwidth is divided into fourteen channels. MB-OFDM uses different channels while sending OFDM packages. Fourteen UWB channels form six channel groups. This is the main difference between MB-OFDM and OFDM [6].

One of the approaches to increase the range of MB-OFDM systems, dual carrier modulation (DCM), was presented in [7] for the first time. In DCM, 4 bits are mapped to two different 16-points constellations. These two symbols are separated by at least 200 MHz in bandwidth. Thus, DCM provides high data rate transmission for longer distances [7]. DCM in single carrier mode was studied in the IEEE 802.11ad channel and gained 1.5dB compared to non-DCM [8]. Outage and BER analysis in the frequency selective channel of DCM for multiband OFDM were derived in [9].

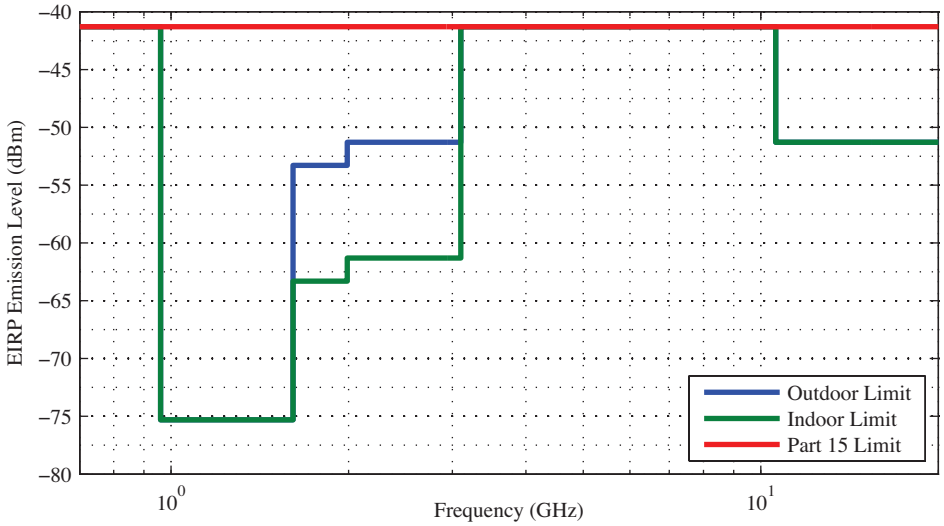

Figure 1. Spectral mask of UWB [1, 2].

In this study, DCM is performed with QPSK. Bit number per symbol is increased by using QPSK instead of 16 QAM in DCM. Therefore, throughput performance is thought to be increased in the BAN channel. QPSK and DCM constellation diagrams are mentioned as mapping diagrams in ECMA-368. The rest of this paper is organized as follows: in Section 2, the basic system model of the DCM is given. The proposed QPSK-DCM model is given in Section 3. In Section 4, the WBAN channel models used in this study are given. Simulation results are presented in Section 5. Theoretical BER and SER performances of QPSK-DCM and 16QAM-DCM are extracted in Section 6. Finally, Section 7 contains conclusions.

2. Dual carrier modulation

In dual carrier modulation, data are split into 200-bit length groups. These bits are divided into 4 groups with different orders, which are dependents on Eqs. (1) and (2) [4]:

$$(I[g(k)], I[g(k)+1], I[g(k)+50], I[g(k)+1+50]), \tag{1}$$

$$g(k) = \begin{cases} 2k, & k \in [0, 24] \\ 2k + 50, & k \in [25, 49], \end{cases} \tag{2}$$

$$M = \begin{bmatrix} I[0] & I[1] & I[50] & I[51] \\ I[2] & I[33] & I[52] & I[53] \\ \dots & \dots & \dots & \dots \\ I[146] & I[147] & I[196] & I[197] \\ I[148] & I[149] & I[198] & I[199] \end{bmatrix}_{50x4}, \tag{3}$$

where $I[\ ]$ is the input data array, $g[\ ]$ is the function used for assigning the sequence of the bits, and M is a matrix consisting of $I[\ ]$ and $g[\ ]$. Elements of M in Eq. (3) are modulated using the 16QAM constellation maps shown in Figures 2a and 2b.

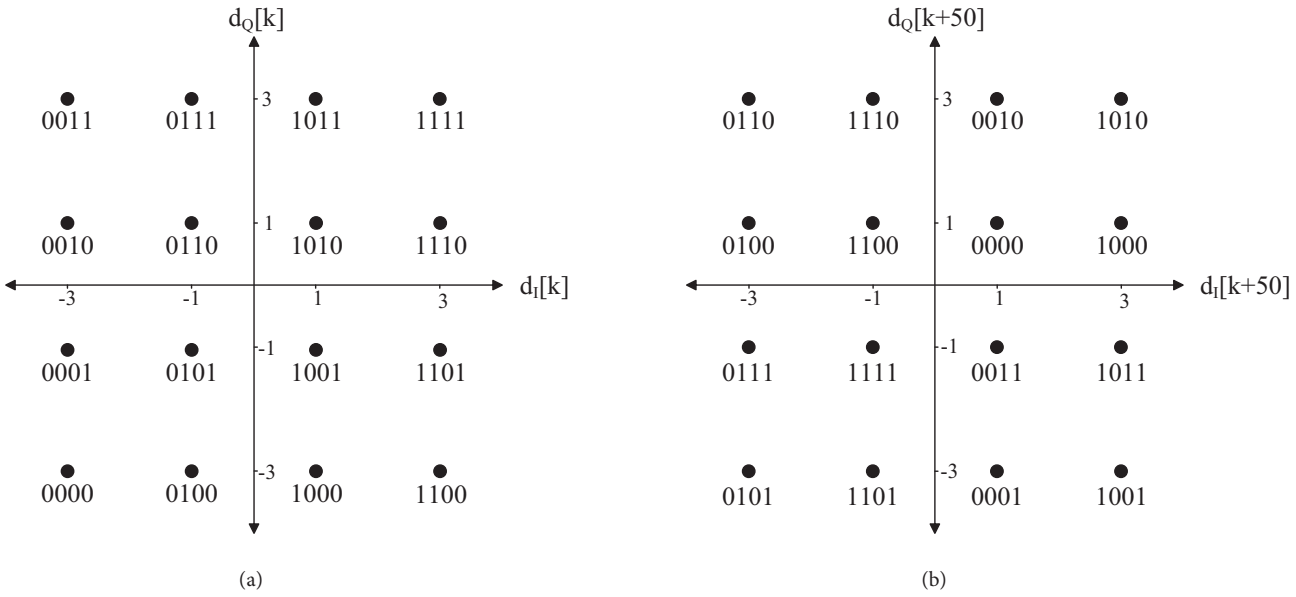

Figure 2. Constellation diagrams of DCM (d_I is real part of 16QAM symbols and d_Q is imaginary part of 16QAM symbols): a) first 50 symbols' constellation diagram, b) second 50 symbols' constellation diagram.

Eventually, 200 bits of data transform to 50 symbols twice and 100 symbols are obtained. The $1/\sqrt{10}$ factor is multiplied with the symbols to normalize the amplitude. Figure 3 shows the block diagram of DCM and the inverse fast Fourier transform (IFFT) part of OFDM [3, 7]. As seen in Figure 3, the first and second 100 bits are divided into 50 bits and 4-bit groups come from first and second 100-bit groups are combined in the constellations diagrams, and two times 50 symbols are obtained. Then IFFT is applied to perform OFDM.

3. QPSK-DCM for BAN channels

DCM is used in ECMA-368 for a higher data rate. After the regular DCM method [7], 32-QAM DCM was introduced in [10] to increase the data rate at 600 Mbps. In the body area network communication, transmission reliability is more important than the data rate. Therefore, the IEEE 802.15.6 standard suggested that the uncoded data rate can be at most 15.6 Mbps [3]. In this study, DCM is applied to IEEE 802.15.6 channel;

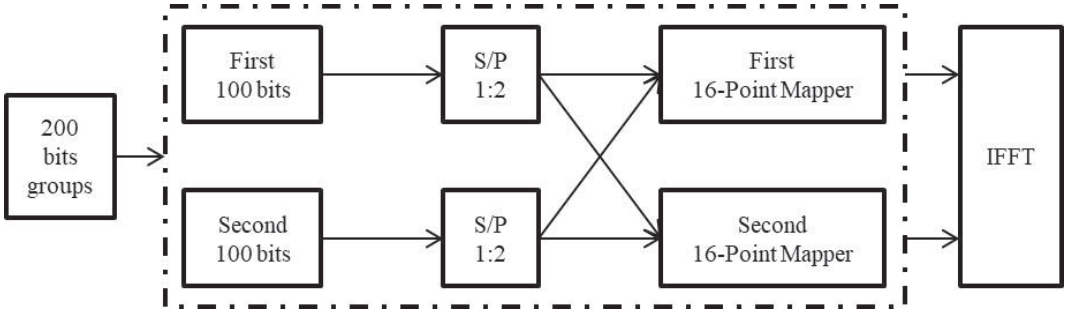

Figure 3. Block diagram of DCM system.

however, code length is kept short and QPSK is used instead of higher orders of QAM types. The aim is to keep the reliability of transmission high while using OFDM and DCM. By proposing the QPSK-DCM, distances between symbols are increased compared to regular 16QAM-DCM.

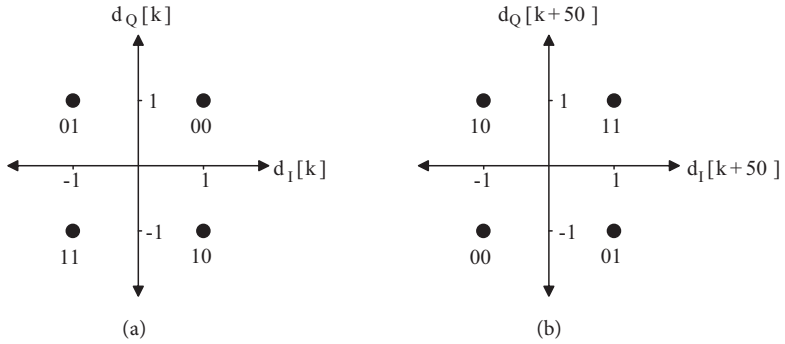

Figure 4. Constellation diagrams of QPKS-DCM: a) first 100 symbols' constellation diagram, b) second 100 symbols' constellation diagram.

Table 1. QPSK-DCM coding table.

Input bits (b[g(k)], b[g(k)+50])	d[k] Q_{out}	d[k] I_{out}	d[k + 50] Q_{out}	d[k + 50] I_{out}
00	1	1	–1	–1
01	1	–1	–1	1
10	–1	1	1	–1
11	–1	–1	1	1

The QPSK constellations are shown in Figure 4 as well as in Table 1. Bits are grouped as 200 bits in 16QAM-DCM. Eqs. (1)–(3) are transformed to Eqs. (4)–(6) to adapt the QPSK-DCM modulation:

$$(I[g(k)], I[g(k)+50]), \tag{4}$$

$$g(k) = \begin{cases} k, & k \in [0, 49] \\ k+50, & k \in [50, 99], \end{cases} \tag{5}$$

$$M = \begin{bmatrix} I[0] & I[50] \\ I[1] & I[51] \\ \dots & \dots \\ I[148] & I[198] \\ I[149] & I[199] \end{bmatrix}_{100x2}, \tag{6}$$

where $I[\ ]$ is the input data array, $g[\ ]$ is the function used for assigning the sequence of the bits, and M is a matrix consisting of $I[\ ]$ and $g[\ ]$. Elements of M in Eq. (6) are modulated using the QPSK constellation maps shown in Figure 4. The $1/\sqrt{2}$ factor is multiplied with the symbols to normalize the amplitude.

Eventually, 200 bits of data transform to 100 symbols twice and 200 symbols are obtained. Then IFFT is applied to perform OFDM. Figure 5 shows the block diagram for QPSK-DCM. Fifty-six pilot symbols are added to 200 data symbols for completion to 256 to keep the IFFT length 2^N and the IFFT is taken.

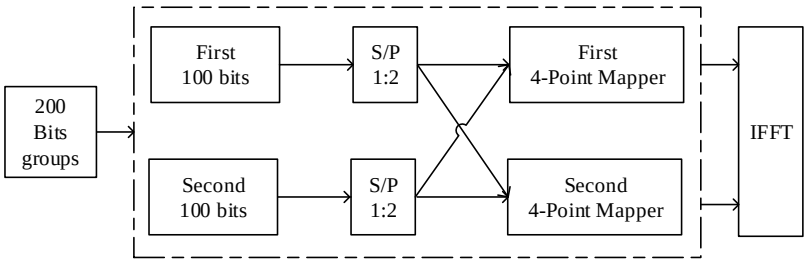

Figure 5. Block diagram of QPSK-DCM system.

4. Channel model

The IEEE 802.15 group published these channel models in 2010 [11]. Among the four BAN channels, channel model 4 (CM4) is used in the simulations. Sensor transmitters are on-body and a hub is out of the body in the CM4. The channel model provides the power delay profile as in Eq. (7):

$$h(t) = \sum_{l=0}^{L-1} a_l e^{-j\phi_l} \delta(t - t_l), \tag{7}$$

where a_l is path amplitude, t_l is arrival time, ϕ_l is phase for path l, and L is the total number of paths. The ϕ_l phase is modeled as uniformly distributed in the $[0, 2\pi]$ interval. a_l is modeled as in Eq. (8):

$$10 \log |a_l|^2 = \begin{cases} 0, & l = 0 \\ \Upsilon_0 + 10 \log e^{-t_1/\Gamma} + S, & l \neq 0, \end{cases} \tag{8}$$

where S is a log-normal modeled stochastic term with zero mean and σ_S is standard derivation. Γ is an exponential distortion constant and Υ_0 is a Rician factor. Arrival time t_l is modeled as Poisson distribution $(p(t_l|t_{l-1}))$ with λ mean time between arrivals as in Eq. (9). The constant is defined in [7] according to model types:

$$p(t_l|t_{l-1}) = \lambda e^{-\lambda(t_l|t_{l-1})}. \tag{9}$$

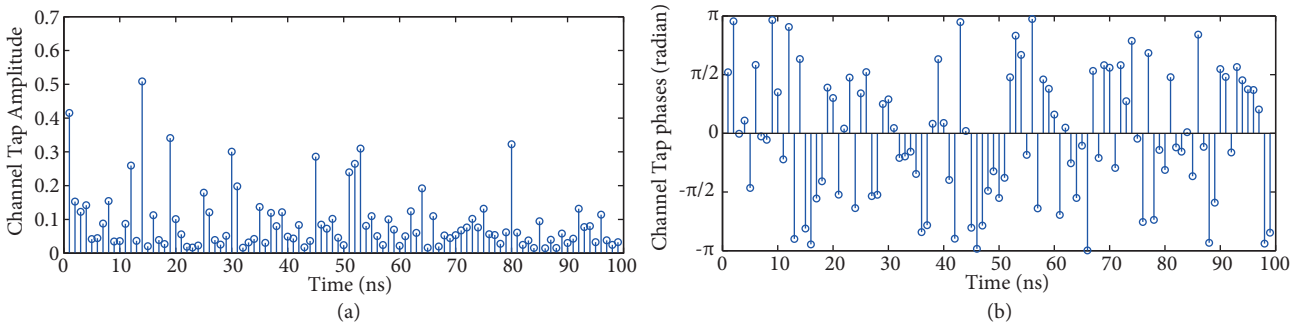

Figure 6. Channel power delay profile of CM4: a) amplitude response, b) phase response.

Figures 6a and 6b show amplitude and phase responses of the channel delay profile of CM4, respectively. This channel model is used in the simulations realized in this study. The angle between the transmitter and receiver is 0° in the model that is used. An average multipath number is chosen as one hundred for CM4 [11]. The same channel models were studied in [12, 13] to analyze equalizer and OFDM performances in BAN channels.

5. Simulations on BAN channel

A block diagram of the simulation model is shown in Figure 7. First, random data are created and applied to the DCM in 200 bits groups. For four DCM data sequences, 800 data symbols and 224 pilot symbols are used. After the modulation AWGN is added to the signal.

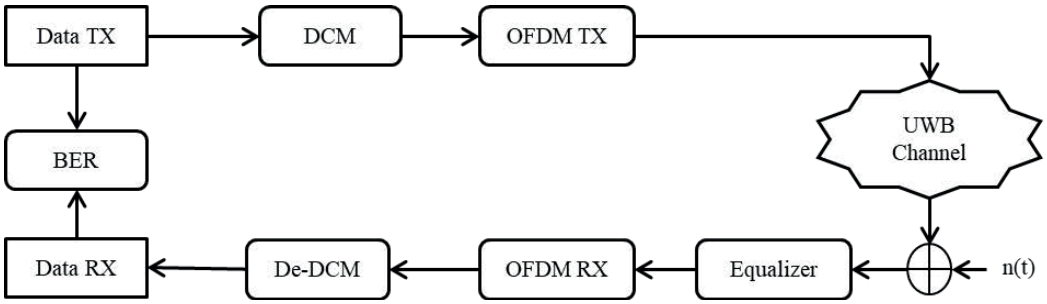

Figure 7. Block diagram of the simulation.

Since the BAN channel multipath number is high, higher pilot symbols are required to struggle with channel distortion effects. Therefore, eight 16QAM-DCM packages or four QPSK-DCM packages are combined as one package, and package size is kept at 1024 bits and pilot symbols number is kept at 224 bits. By adding the cyclic prefix (CP), the OFDM transmitter is achieved. In the OFDM receiver, the received signal contains the destructive transmitted signal, channel effect, and AWGN. A zero forcing equalizer [12, 14] as in Eqs. (10) and (11) is applied in the OFDM receiver to avoid the channel effect. By the pilot symbols, the channel impulse response is detected and the equalizer is derived from the impulse response:

$$R = \rho H + n, \tag{10}$$

$$\hat{H} = R/\rho, \tag{11}$$

where R is the received signal, n is AWGN, $\hat{H}$ is the estimated channel, and ρ is the pilot symbol. Here, the AWGN is neglected. The output of the filter is interpolated by linear interpolation method to estimate the channel at data subcarriers [12].

Demodulation of DCM is realized by the comparison of the received symbol to two constellation diagrams. Therefore, the sums of the absolute difference of the received symbol and modulation symbols are calculated as in Eq. (12), and the smallest one is chosen as the received modulation symbol:

$$min(\sum \mid \hat{R}_{DCM} - R_{DCM} \mid), \tag{12}$$

where $\hat{R}_{DCM}$ is the received DCM signal obtained in the OFDM receiver and R_{DCM} represents DCM symbols.

Figures 8a and 8b show QPSK-DCM, QPSK-OFDM, 16QAM-DCM, and 16QAM-OFDM performances in CM4 with a 0° angle between the transmitter and receiver. Among these modulations, QPSK-DCM shows the best performance in the 100-paths BAN channel. When OFDM symbol quantity is increased to 2048 with the same pilot symbol ratio, Figures 9a and 9b are obtained from simulations. In both figures, 'a' shows the performance without considering the double symbol in the DCM situation in which the same data symbol is sent twice, and 'b' shows the performance considering the double symbol in DCM. Therefore, there is 3 dB difference between 'a' and 'b' in Figures 8 and 9. Since the pilot amount is raised, better performances (about 10 dB difference) are obtained in 16QAM-DCM, QPSK-OFDM, and 16QAM-OFDM. Using more pilot symbols improves the performance in DCM-OFDM simulation, but it was not sufficient to avoid the error floor. To reduce the error floor, pilot symbol and cyclic prefix quantities can be increased and different channel coding techniques such as low-density parity-check (LDPC) can be used.

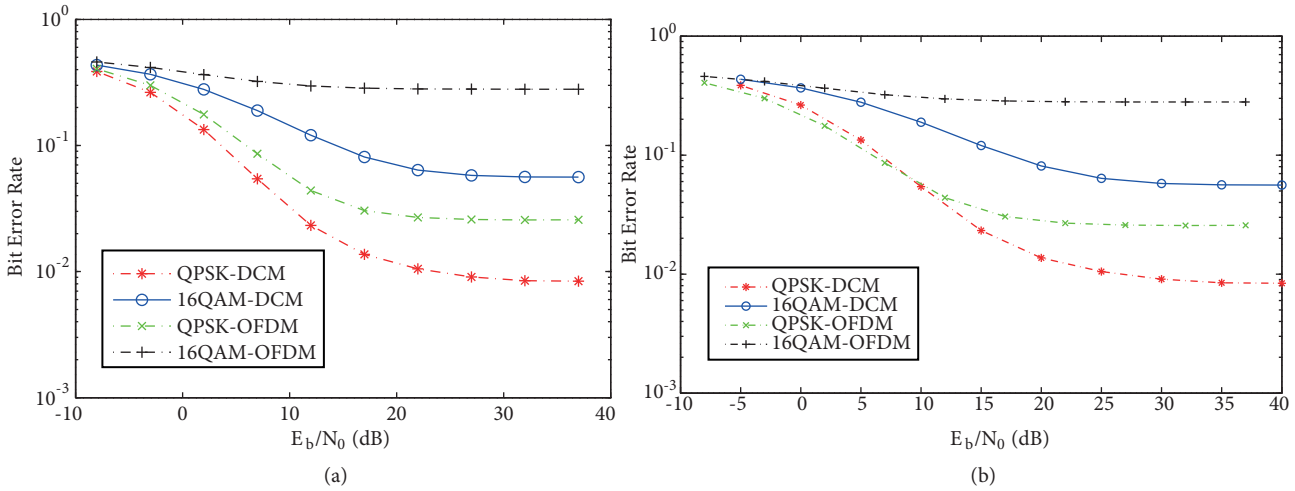

Figure 8. Performance graph of DCM and OFDM modulations in BAN channel (1024 OFDM symbols): a) without considering double symbol in DCM, b) considering double symbol in DCM.

6. Theoretical error rates calculations in AWGN channel

In this section theoretical bit and symbol error rates for QPSK-DCM and 16QAM-DCM are extracted and compared with simulations. Extracted formulas and the simulation results coincide with each other.

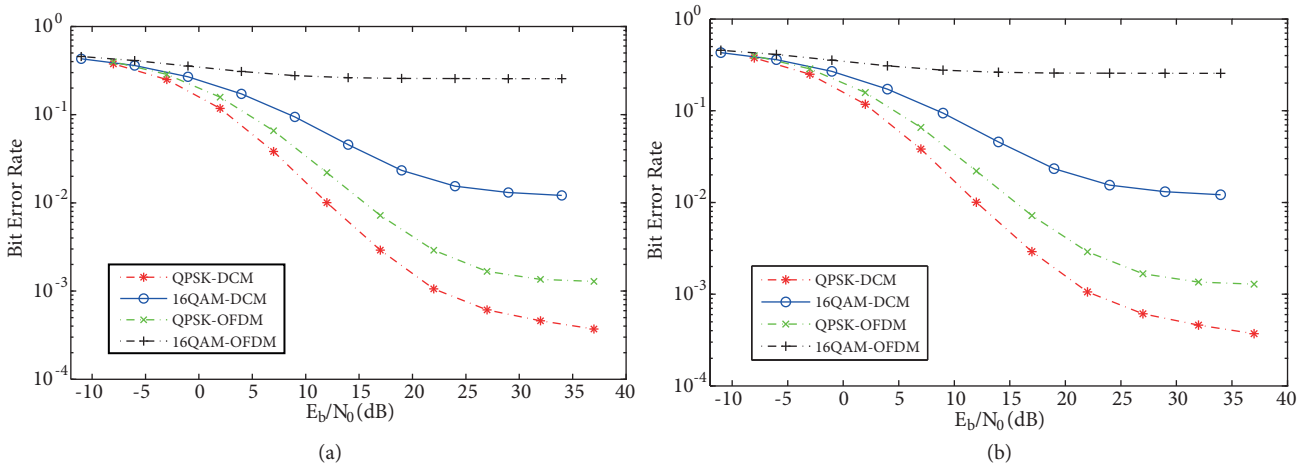

Figure 9. Performance graph of DCM and OFDM modulations in BAN channel (2048 OFDM symbols): a) without considering double symbol in DCM, b) considering double symbol in DCM.

6.1. Error rates calculations for QPSK-DCM in AWGN channel

Symbol and bit error rates of QPSK are $erfc(\sqrt{E_s/2N_0})$ and $1/2erfc(\sqrt{(E_b/N_0)})$, respectively [15]. Since two different QPSK constellation diagrams are used in QPSK-DCM for the same bits, BER and SER differ from regular QPSK. To demodulate QPSK-DCM, two QPSK demodulations are realized and compared to the DCM diagram. According to the minimum distance between the received symbol and DCM symbols as in Eq. (13), the received DCM symbol is determined:

$$min(\sum |DCM_{diagram} - RX_{data}|). \tag{13}$$

$DCM_{diagram}$ denotes data in Table 2 and RX_{data} refers to data in the output of OFDM demodulation. The minimum distance of received data to QPSK-DCM data in Table 1 defines the demodulated QPSK-DCM symbol. The four bits should be processed at the same time. If two QPSK symbols are processed separately, lower performance rates are obtained.

Figure 10 shows error areas in I and Q phases of a symbol in the QPSK constellation diagram in the AWGN channel. By obtaining I and Q phases independent from each other, the BER is $1/2erfc(\sqrt{E_b/N_0})$ or $1/2erfc(\sqrt{E_s/2N_0})$ and SER is approximately $erfc(\sqrt{E_s/2N_0})$ in QPSK [15]. To make a theoretical calculation of QPSK-DCM, all possible situations in Eq. (13) should be extracted. The cases for the I phase are shown in Table 2. This table shows received cases of a symbol that is modulated with two different constellation diagrams. Also, it shows which phase is chosen based on the minimum distance. A similar table is available for the Q phase.

Figures 11a and 11b show the I phase of a QPSK-DCM symbol's possible error areas under AWGN channel. Results for cases 0, 1, 4, and 6 in Table 2 are false cases, so they cause error at the receiver and the other results are true cases. Cases 0 and 4 coincide with the A and D regions in Figure 11. Case 1 coincides with regions A and E–F, and Case 6 coincides with regions B–C and D in Figure 11.

According to Figure 11, the bit error rate in the I phase in QPSK-DCM is calculated as in Eq. (14):

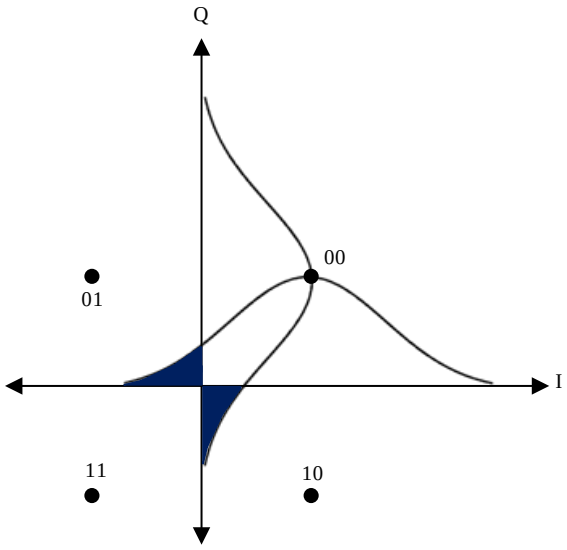

Figure 10. Error areas of a symbol in QPSK constellation diagram.

Table 2. Cases of received I phase in QPSK-DCM receiver.

Case	I(k)	I(k+50)	d(I(k)) < d(I(k+50))	Decision	Result	Probability calculation
0	F	F	T	I(k)	F	$1/2erfc(\sqrt{(E_s/2N_0)})$.
						$1/2erfc(\sqrt{(E_s/2N_0)}).Pr(z_0)$
1	F	T	T	I(k)	F	$1/2erfc(\sqrt{(E_s/2N_0)})$.
						$1/2erfc(\sqrt{(E_s/2N_0)}).(1+Pr(z_1))$
2	T	F	T	I(k)	T	
3	T	T	T	I(k)	T	
4	F	F	F	I(k+50)	F	$1/2erfc(\sqrt{(E_s/2N_0)})$.
						$1/2erfc(\sqrt{(E_s/2N_0)}).Pr(z_0')$
5	F	T	F	I(k+50)	T	
6	T	F	F	I(k+50)	F	$1/2erfc(\sqrt{(E_s/2N_0)})$.
						$1/2erfc(\sqrt{(E_s/2N_0)}).(1+Pr(z_1'))$
7	T	T	F	I(k+50)	T	

$$Pr(BER)_{QPSK-DCM} = 1/2erfc(\sqrt{E_s/2N_0}).1/2erfc(\sqrt{E_s/2N_0}).Pr(d(I(k)) < d(I(k+50)) \mid \{d(I(k)) \in A \& d(I(k+50)) \in D\}) + 1/2erfc(\sqrt{E_s/2N_0}).1/2erfc(\sqrt{E_s/2N_0}).Pr(d(I(k)) > d(I(k+50)) \mid \{d(I(k)) \in A \& d(I(k+50)) \in D\}) + 1/2erfc(\sqrt{E_s/2N_0}).1/2erfc(\sqrt{E_s/2N_0}).(Pr(d(I(k)) < d(I(k+50)) \mid \{d(I(k)) \in A \& d(I(k+50)) \in E\})) + 1/2erfc(\sqrt{E_s/2N_0}).\quad (14)$$
$$1/2erfc(\sqrt{E_s/2N_0}).(Pr(d(I(k)) < d(I(k+50)) \mid \{d(I(k)) \in A \& d(I(k+50)) \in F\})) + 1/2erfc(\sqrt{E_s/2N_0}).1/2erfc(\sqrt{E_s/2N_0}).(Pr(d(I(k)) > d(I(k+50)) \mid \{d(I(k)) \in B \& d(I(k+50)) \in D\})) + 1/2erfc(\sqrt{E_s/2N_0}).1/2erfc(\sqrt{E_s/2N_0}).(Pr(d(I(k)) > d(I(k+50)) \mid \{d(I(k)) \in C \& d(I(k+50)) \in D\})).$$

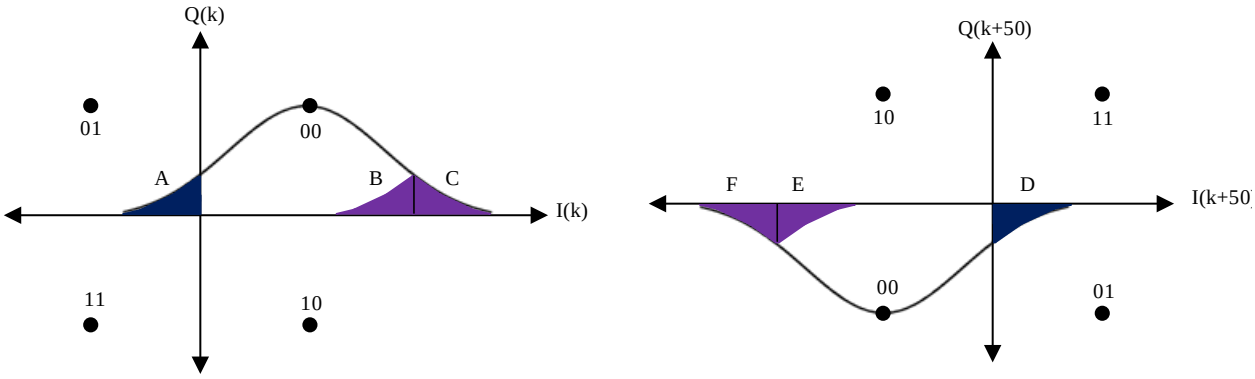

Figure 11. Two QPSK constellation diagrams suited to QPSK-DCM: a) for b[g(k)], b) for b[g(k)+50].

The calculation of probability equations in Eq. (14) is given in Eqs. (15)–(17):

$$Pr(d(I(k)) < d(I(k+50)) \mid \{d(I(k)) \in A \& d(I(k+50)) \in D\}) + Pr(d(I(k)) > d(I(k+50)) \mid \{d(I(k)) \in A \& d(I(k+50)) \in D\}) = 1, \tag{15}$$

$$(Pr(d(I(k)) < d(I(k+50)) | \{d(I(k)) \in A \& d(I(k+50)) \in F\})) - (Pr(d(I(k)) > d(I(k+50)) \mid \{d(I(k)) \in C \& d(I(k+50)) \in D\})) = 1, \tag{16}$$

$$(Pr(d(I(k)) < d(I(k+50)) | \{d(I(k)) \in A \& d(I(k+50)) \in E\})) + (Pr(d(I(k)) > d(I(k+50)) \mid d(I(k)) \in B \& d(I(k+50)) \in D)) = 1. \tag{17}$$

At a result, the bit error rate of a symbol of QPSK-DCM is given in Eq. (18). Since the probability of sending each symbol is the same, Eqs. (18) and (19) give the BER of QPSK-DCM:

$$Pr(BER)_{QPSK-DCM} = 1/2erfc(\sqrt{E_s/2N_0}).1/2erfc(\sqrt{E_s/2N_0}).4 = erfc^2(\sqrt{E_s/2N_0}), \tag{18}$$

$$Pr(BER)_{QPSK-DCM} = 4.(Pr(BER)_{QPSK})^2. \tag{19}$$

The symbol error rate of QPSK-DCM is defined in Eqs. (20) and (21):

$$Pr(SER)_{QPSK-DCM} = 1 - (1 - Pr(BER)_{QPSK-DCM})^2 = 2Pr(BER)_{QPSK-DCM} - Pr(BER)^2_{QPSK-DCM}, \tag{20}$$

$$Pr(SER)_{QPSK-DCM} = 2erfc^2(\sqrt{E_s/2N_0}) - erfc^4(\sqrt{E_s/2N_0}) \approx 2erfc^2(\sqrt{E_s/2N_0}). \tag{21}$$

Figure 12a and 12b show the bit and symbol error rates simulation results and obtained theoretical equations for QPSK-DCM. Also, the QPKS performance result is shown in the same figure. Figure 12a shows

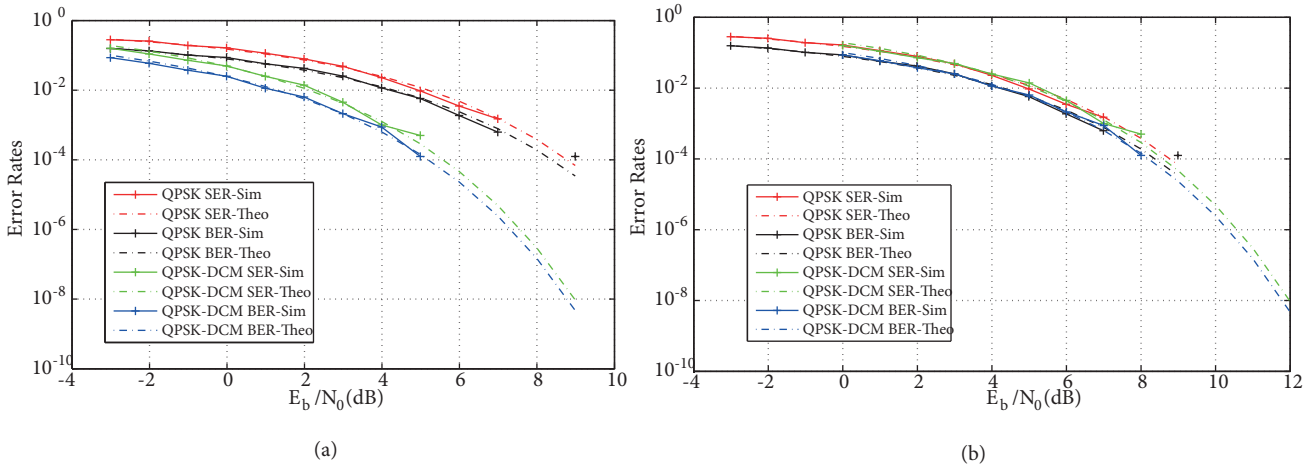

Figure 12. Theoretical and simulation results for QPSK and QPSK-DCM: a) without considering double symbol in DCM, b) considering double symbol in DCM.

the performance without considering the double symbol in the DCM situation in which the same data symbol is sent twice, and Figure 12b shows performance considering the double symbol in DCM. From Figure 12, it is seen that simulation results and obtained theoretical equations for the bit and symbol error rates are close to each other.

6.2. Error rates calculations for DCM in AWGN channel

To analyze 16QAM error rates in DCM, 4 dimensions' calculations are used. Figures 13a and 13b show two 16QAM constellation diagrams used in DCM and Table 3 shows DCM symbols. Figure 13 also shows possible error areas for the symbol '0000' for both constellations used in DCM as well. Table 4 shows possible received symbols when the DCM symbol '0000' is sent.

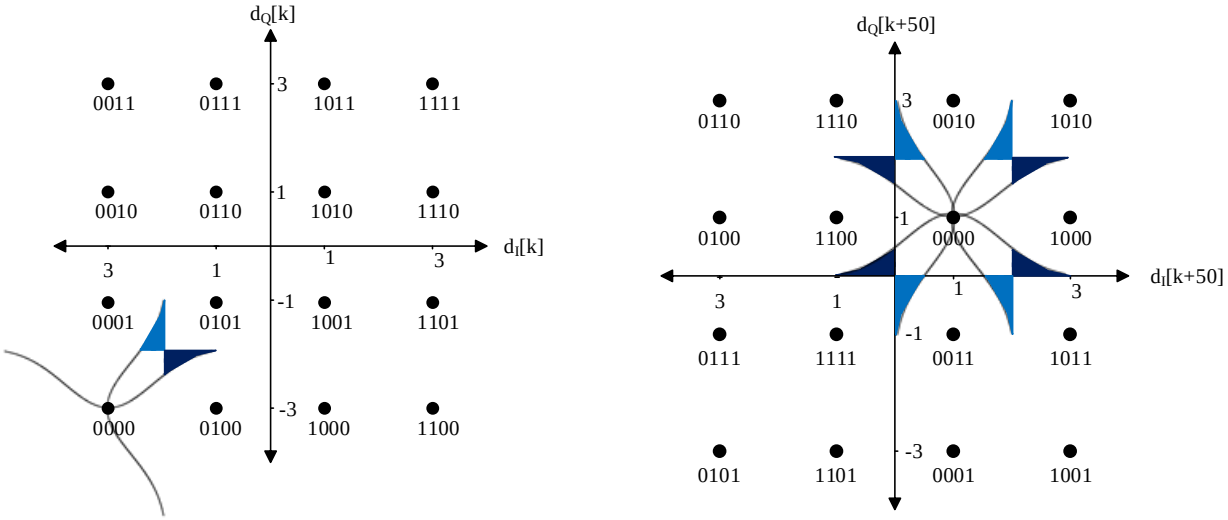

Figure 13. Two constellation diagrams of 16QAM used in DCM: a) b[g(k)] input array, b) b[g(k)+50] input array.

Table 3. DCM coding table.

Input bits (b[g(k)], b[g(k)+1], b[g(k) + 50], b[g(k) + 51])	d[k] I_{out}	d[k] Q_{out}	d[k + 50] I_{out}	d[k + 50] Q_{out}
0000	−3	−3	1	1
0001	−3	–1	1	−3
0010	−3	1	1	3
0011	−3	3	1	–1
0100	−1	−3	−3	1
0101	−1	–1	−3	−3
0110	−1	1	−3	3
0111	−1	3	−3	–1
1000	1	−3	3	1
1001	1	–1	3	−3
1010	1	1	3	3
1011	1	3	3	–1
1100	3	−3	–1	1
1101	3	–1	–1	−3
1110	3	1	–1	3
1111	3	3	–1	–1

When the symbol '0000' is sent, possible received symbols are compared to the original symbol '0000' to extract the error rate. Therefore, cases 10–11, 13–14, 16–17, and 21–35 in Table 4, which are a total of 20 cases, are possible error received symbols when '0000' is sent. Among these cases, just two DCM bits are wrong in cases 10, 11, 21, and 24. The probability of realization of each of these four cases is as follows:

$$\begin{aligned}&\left(1-Q\left(\sqrt{\frac{E_s}{10N_0}}\right)\right).Q\left(\sqrt{\frac{E_s}{10N_0}}\right).\left(1-Q\left(\sqrt{\frac{E_s}{10N_0}}\right)\right).Q\left(\sqrt{\frac{E_s}{10N_0}}\right)\\&\qquad=Q\left(\sqrt{\frac{E_s}{10N_0}}\right)^2-2Q\left(\sqrt{\frac{E_s}{10N_0}}\right)^3+Q\left(\sqrt{\frac{E_s}{10N_0}}\right)^4.\end{aligned}\tag{22}$$

Additionally, three DCM bits are wrong in cases 13–14, 16–17, 23, and 25–35. The probability of realization of each of these four cases is:

$$\left(1-Q\left(\sqrt{\frac{E_s}{10N_0}}\right)\right).Q\left(\sqrt{\frac{E_s}{10N_0}}\right).Q\left(\sqrt{\frac{E_s}{10N_0}}\right).Q\left(\sqrt{\frac{E_s}{10N_0}}\right)=Q\left(\sqrt{\frac{E_s}{10N_0}}\right)^3-Q\left(\sqrt{\frac{E_s}{10N_0}}\right)^4.\tag{23}$$

Thus, the symbol error rate for symbol '0000' is:

$$Pr(SER)_{DCM-1symbol}=4Q\left(\sqrt{\frac{E_s}{10N_0}}\right)^2+8Q\left(\sqrt{\frac{E_s}{10N_0}}\right)^3-12Q\left(\sqrt{\frac{E_s}{10N_0}}\right)^4.\tag{24}$$

The same equation is found for other DCM symbols. Each DCM symbol has 10 error areas in two 16QAM constellation diagrams as in Figure 13. Similar to Table 4, the other symbol's possible received cases are

Table 4. Possible received symbols when DCM symbol '0000' is sent.

Case	d[k] I_{out}	d[k] Q_{out}	d[k + 50] I_{out}	d[k + 50] Q_{out}	Case	d[k] I_{out}	d[k] Q_{out}	d[k + 50] I_{out}	d[k + 50] Q_{out}
0	–3	–3	1	1	18	–1	–3	1	1
1	–3	–3	1	–1	19	–1	–3	1	–1
2	–3	–3	1	3	20	–1	–3	1	3
3	–3	–3	–1	1	21	–1	–3	–1	1
4	–3	–3	–1	–1	22	–1	–3	–1	–1
5	–3	–3	–1	3	23	–1	–3	–1	3
6	–3	–3	3	1	24	–1	–3	3	1
7	–3	–3	3	–1	25	–1	–3	3	–1
8	–3	–3	3	3	26	–1	–3	3	3
9	–3	–1	1	1	27	–1	–1	1	1
10	–3	–1	1	–1	28	–1	–1	1	–1
11	–3	–1	1	3	29	–1	–1	1	3
12	–3	–1	–1	1	30	–1	–1	–1	1
13	–3	–1	–1	–1	31	–1	–1	–1	–1
14	–3	–1	–1	3	32	–1	–1	–1	3
15	–3	–1	3	1	33	–1	–1	3	1
16	–3	–1	3	–1	34	–1	–1	3	–1
17	–3	–1	3	3	35	–1	–1	3	3

extracted. Each symbol has the same possibility of occurrence. Thus, the DCM modulation symbol error rate is the same as one of the symbol's SER as in Eq. (24). However, these calculations are made for the DCM symbol, and the DCM symbol's energy is twice the 16QAM symbol energy: $E_{s-DCM} = 2E_s$. Thus, the final SER of DCM under an AWGN channel should be as in Eq. (25). Eq. (26) shows the SER of DCM with erfc function:

$$Pr(SER)_{DCM} = 4Q\left(\sqrt{\frac{2E_s}{10N_0}}\right)^2 + 8Q\left(\sqrt{\frac{2E_s}{10N_0}}\right)^3 - 12Q\left(\sqrt{\frac{2E_s}{10N_0}}\right)^4, \tag{25}$$

$$Pr(SER)_{DCM} = 2erfc\left(\sqrt{\frac{2E_s}{10N_0}}\right)^2 + 4erfc\left(\sqrt{\frac{2E_s}{10N_0}}\right)^3 - 6erfc\left(\sqrt{\frac{2E_s}{10N_0}}\right)^4. \tag{26}$$

From this equation, the bit error rate is a quarter of the SER:

$$Pr(BER)_{DCM} \approx \frac{Pr(SER)_{DCM}}{4} = 0.5erfc\left(\sqrt{\frac{2E_s}{10N_0}}\right)^2 + erfc\left(\sqrt{\frac{2E_s}{10N_0}}\right)^3 - 1.5erfc\left(\sqrt{\frac{2E_s}{10N_0}}\right)^4. \tag{27}$$

Theoretical and simulation SER and BER performance results of 16QAM-DCM are shown in Figure 14. Figure 14a shows the performance without considering the double symbol in the DCM situation, which is the same data symbol sent twice, and Figure 14b shows the performance considering the double symbol in DCM. Simulation and the extracted theoretical results are close to each other, as seen in these figures.

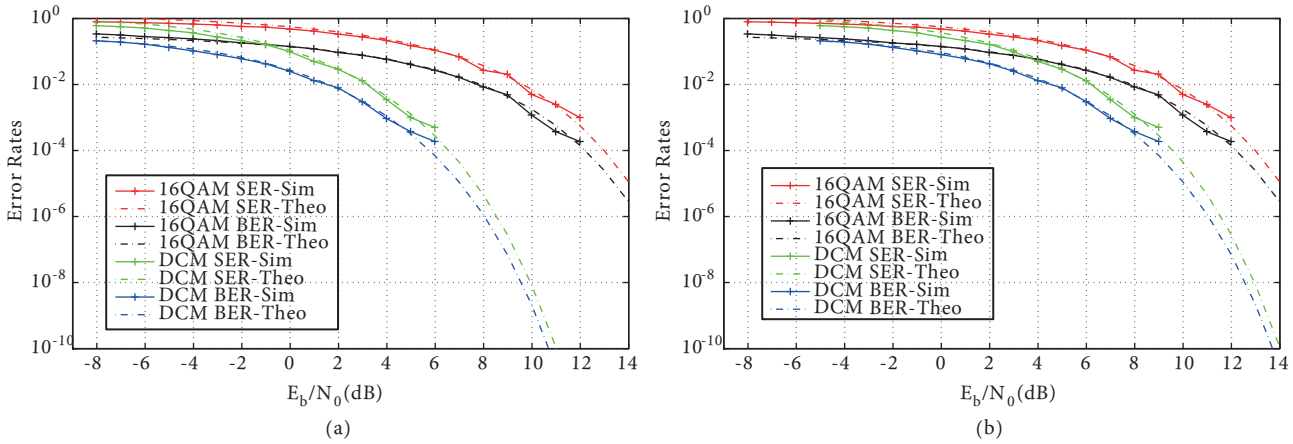

Figure 14. Theoretical and simulation results for 16QAM and 16QAM-DCM: a) without considering double symbol in DCM, b) considering double symbol in DCM.

7. Conclusion

In this study, QPSK-DCM is analyzed and compared with QPSK-OFDM, 16QAM-OFDM, and 16QAM-DCM in a wireless body area network channel. The channel performance is more important than data rate in WBAN channels. Therefore, QPSK-DCM is proposed to be used in 2 bits per symbol instead of 4 bits symbols to improve the quality of the transmission. The results demonstrate that QPSK-DCM has better error rate performances compared to QPSK-OFDM, 16QAM-DCM, and 16QAM-OFDM. Also, the same simulation is realized with higher pilot data and performance increases are seen as pilot quantity increases. Additionally, the theoretical BER and SER in the AWGN channel are extracted for QPSK-DCM and 16QAM-DCM modulations. Even though the QPSK-DCM energy per bit to noise power spectral density ratio (E_b/N_0) performance seems nearly equal to QPSK E_b/N_0 performance, apparently QPSK-DCM shows better performance among others in the WBAN channel.

References

[1] Sahinoglu Z, Gezici S, Guvenc I. Ultra-wideband Positioning Systems: Theoretical Limits, Ranging Algorithms, and Protocols. New York, NY, USA: Cambridge University Press, 2008. doi: 10.1017/CBO9780511541056

[2] Zhang J, Orlik PV, Sahinoglu Z, Molisch AF, Kinney P. UWB systems for wireless sensor networks. Proceedings of the IEEE 2009; 97 (2): 313-331. doi: 10.1109/JPROC.2008.2008786

[3] IEEE Standards Association. IEEE Standard for Local and Metropolitan Area Networks—Part 15.6: Wireless Body Area Networks. IEEE Std. 802.15.6. New York, NY, USA: IEEE, 2012. doi: 10.1109/IEEESTD.2012.6161600

[4] ECMA International. ECMA-368 High Rate Ultra Wideband PHY and MAC Standard. ECMA Std. Geneva, Switzerland: ECMA, 2008.

[5] Batra A, Balakrishnan J, Dabak A, Gharpurey R, Lin J et al. Physical layer submission to 802.15 task group 3a: Multi-band orthogonal frequency division multiplexing. IEEE P802.15 Working Group for Wireless Personal Area Networks (WPANs). New York, NY, USA: IEEE, 2004.

[6] Batra A, Balakrishnan J, Aiello GR, Foerster JR, Dabak A. Design of a multiband OFDM system for realistic UWB channel environments. IEEE Transactions on Microwave Theory and Techniques 2004; 52 (9): 2123-2138. doi: 10.1109/TMTT.2004.834184

[7] Batra A, Balakrishnan J. Improvements to the multi-band OFDM physical layer. In: Consumer Communications and Networking Conference; Las Vegas, NV, USA; 2006. pp. 701-705. doi: 10.1109/CCNC.2006.1593129

[8] Wu T, Chen T. Dual carrier modulation in channel aggregation for 60GHz WLAN System. IEEE Wireless Communications Letters 2018; 7 (4): 792-795. doi: 10.1109/LWC.2018.2825434

[9] Kondoju SK, Mani VV. Outage and BER analysis of dual-carrier modulation over frequency-selective Nakagami-m fading channels. COMPEL-The International Journal for Computation and Mathematics in Electrical and Electronic Engineering 2017; 36 (1): 90-107. doi: 10.1108/COMPEL-03-2016-0097

[10] Yang R, Sherratt RS. Multiband OFDM Modulation and Demodulation for Ultra Wideband Communications. Rijeka, Croatia: Intech Open Publishing, 2011. doi: 10.5772/16700

[11] Yazdandoost K, Sayrafian-Pour K. TG6 Channel Model ID: 802.15-08-0780-12-0006. New York, NY, USA: IEEE, 2010.

[12] Karan Y, Şaylı O, Kahveci S. OFDM Performance of ultra wideband in wireless body area network channel. Acta Physica Polonica A 2017; 132 (3): 574-576. doi: 10.12693/APhysPolA.131.574

[13] Karan Y, Kahveci S. LMS and RLS equalizer performances of ultra wideband system in body area network channel. In: Signal Processing and Communication Application Conference; Zonguldak, Turkey; 2016. pp. 285-288. doi: 10.1109/SIU.2016.7495733

[14] Wang JB, Jiao Y, Dang XY, Chen M, Xie XX et al. Training sequence based channel estimation for indoor visible light communication system. Optoelectronics Letters 2011; 7 (3): 213-216. doi: 10.1007/s11801-011-0143-7

[15] Barry JR, Lee EA, Messerschmitt DG. Digital Communication. New York, NY, USA: Springer Science & Business Media, 2004. doi: 10.1007/978-1-4615-0227-2